

New insights into the photo-enhanced electrocatalytic reduction of carbon dioxide on MoS₂-rods/TiO₂ NTs with unmatched energy band

Peiqiang Li*, Haitao Hu, Jinfeng Xu, Hua Jing, Hui Peng, Jing Lu, Chenxiao Wu, Shiyun Ai*

College of Chemistry and Material Science, Shandong Agricultural University, 271018, PR China

ARTICLE INFO

Article history:

Received 6 July 2013

Received in revised form 3 October 2013

Accepted 7 October 2013

Available online 15 October 2013

Keywords:

MoS₂-rods/TiO₂ NTs

PEEC reduction

Carbon dioxide

Ethanol

ABSTRACT

In this paper, the highly-ordered TiO₂ nanotube arrays (TiO₂ NTs) were obtained by improved anodic oxidation method and the MoS₂-rods were assembled to the TiO₂ NTs by a facile hydrothermal method, obtained the MoS₂-rods/TiO₂ NTs heterojunction. According to the UV-vis DRS and XPS analysis, the obtained MoS₂-rods/TiO₂ NTs exhibited excellent absorption in the visible area (400–600 nm) and its energy band gap was 1.55 eV, but its conduction band (−0.15 eV) was more positive than the CO₂ reduction potential, it indicated that MoS₂-rods/TiO₂ NTs had no ability for photocatalytic reduction of CO₂. Electrocatalysis could reduce CO₂, but the products yield was very low and the faraday efficiency gradually reduced with reaction going on. Interestingly, when illumination was introduced into the electrocatalytic process, the light greatly enhanced the CO₂ electrocatalytic reduction ability of the MoS₂-rods/TiO₂ NTs. Furthermore, the faraday efficiency increased to 2.65 times from 42.20% (electrocatalysis) to 111.58% (photo-enhanced electrocatalysis), and the methanol yield increased to 2.29 times from 6.32 mmol L^{−1} to 14.49 mmol L^{−1}. The new insights for how light enhanced electrocatalytic reduction of CO₂ was elaborated systematically from three aspects, that is, reduction overpotential, enhanced electron transmission ability, and generated p-n heterojunction. Furthermore, the generation mechanism of methanol with photo-enhanced electrocatalysis was also deduced. Especially, we deduced that the protons involving into the CO₂ reduction came from two aspects, one was from the electrocatalytic oxidation water on the anode, and the other was from the in situ photocatalytic oxidation water on the cathode.

© 2013 Elsevier B.V. All rights reserved.

1. Introduction

Over the past decades, the atmospheric concentration of CO₂ has been increasing rapidly owing to the expanded human activity, which consequently has accelerated the greenhouse effect and brings a series of hazard. As an inexpensive, nontoxic and abundant C1 feedstock, many ideas have involved in trapping the “greenhouse gas” and converting it into fuels or organic materials using renewable energy [1]. To date, methods including chemical absorption, physical adsorption, bioconversion, photocatalytic reduction and electrocatalytic reduction have been investigated for CO₂ sequestrations. Among them, the photocatalytic (PC) reduction and electrocatalytic (EC) reduction are not only clean and environmental friendly for renewable energy, but also high efficiency processing techniques for CO₂ catalytic reduction. Additionally, they also have been known for producing a variety of useful products. For example, under different light intensity and potentials,

compounds such as CH₄, HCOOH, CO and CH₃OH have been synthesized with various yields [1–6]. Among all the products, CH₃OH is the most desired reduction product from CO₂, because it can be easily transported, stored and used directly as gasoline for automobiles. Moreover, methanol can be transformed into other useful chemicals using conventional chemical technologies. Therefore, the selective and efficient conversion of CO₂ to methanol has attracted much research interest.

As a solar energy based technology, photocatalysis has received a good deal of attention. TiO₂ has been widely used in the photocatalysis for its strong redox ability, low cost, stability, and environmental friendly [2–4]. Compared with TiO₂ nanoparticles and nanofilms, TiO₂ nanotubes (TiO₂ NTs) have larger specific surface area, more active sites and higher catalytic activity, so they get more attention [7]. However, the absorption edge of TiO₂ falls in the UV region, which involves only 4% of the sunlight spectrum. The modification of TiO₂ with inorganic substances, such as noble metals, transition metals, non-metals and semiconductors, has been considered for inducing a red shift by decreasing the band gap or introducing intraband gap states, which result in an enhancement of visible light absorption and maximizing its PC efficiency [2,8]. As an earth abundant and nontoxic material, MoS₂ has an appropriate band gap (approximately 1.17 eV), which is small

* Corresponding authors at: College of Chemistry and Material Science, Shandong Agricultural University, 61 Daizong Road, Tai'an, Shandong 271018, PR China.
Tel.: +86 0538 8249017.

E-mail addresses: chem.carbon@outlook.com, pqli@sda.edu.cn (P. Li).

enough to narrow TiO_2 band gap to increase the activity of TiO_2 by extending the wavelength response range of TiO_2 to the visible region [8–10]. However, the conduction band minimum (CBM) of TiO_2 (-0.29 eV) and MoS_2 (-0.15 eV) are both more positive than the reduction potential of CO_2/CH_4 (-0.24 V), $\text{CO}_2/\text{CH}_3\text{OH}$ (-0.38 V), CO_2/HCHO (-0.48 V), CO_2/CO (-0.53 V), $\text{CO}_2/\text{HCO}_2\text{H}$ (-0.61 V) [8,11]. This indicates that no matter how to coupling TiO_2 NTs with MoS_2 the hybrid nanostructured material has no enough reductive ability for PC reduction of CO_2 .

The EC reduction of CO_2 is of growing interest. It directly controls the surface free energy of the catalyst through the electrode potential, allowing the reaction rate and pathway selectivity to be controlled precisely [12,13]. Besides, it does not need to consider energy band matching. MoS_2 has been commonly investigated as a electrocatalyst due to its catalytic activity over a wide range of pH solutions (from pH 0 to pH 13) with a relatively low overvoltage requirement [14–16]. In particular, MoS_2 -based catalysts exhibit a better selectivity to alcohols than other catalysts (e.g. Rh-based and Cu-based catalysts) for alcohols synthesis [9]. Although many studies have used electrocatalysis for conversion and utilization of CO_2 , there are still limitations within such systems, that is the faraday efficiency will gradually reduce with the reaction going on [17].

To address these limitations, we notice that the material not only has excellent EC performance, but also has superior photochemical performance. We expect to overcome the faraday efficiency decline by virtue of the photochemical properties of the material itself. In this study, we used a simple method for coupling the co-catalyst MoS_2 with TiO_2 NTs to obtain the heterojunction (MoS_2 -rods/ TiO_2 NTs) with good photochemical properties, but it cannot reduce CO_2 with individual photocatalysis. The MoS_2 -rods/ TiO_2 NTs was explored as the cathode for EC reducing CO_2 to CH_3OH , but the yield was very low and the faraday efficiency gradually reduced. Adding illumination into the EC systems not only protect the active-sites and aggrandize the faraday efficiency, but also utilize the most abundant sources of energy and hydrogen, being sunlight and water, respectively. We exploited photo-enhanced electrocatalytic (PEEC) reduction of CO_2 to methanol in aqueous solution. Compared with single electrocatalysis, the PEEC showed superior activity in the reduction of CO_2 to CH_3OH . The reasons for the as-prepared MoS_2 -rods/ TiO_2 NTs with superior activity in the PEEC reduction of CO_2 were systematically investigated. And most of all, this study provided great guidance and theory significance for those catalysts with narrow energy band gap and unmatched CBM PEEC reduction of CO_2 .

2. Materials and methods

2.1. Preparation of titania nanotube arrays

Highly ordered TiO_2 NTs were fabricated through anodic oxidation of Ti substrates. The electrolytes were consisted of NH_4F (0.5 wt%), glycol (97.7 wt%) and distilled water (1.8 wt%). The potentiostatic anodic oxidation was performed under 60 V for 60 min at room temperature. After sonicating for 5 min, the samples were put in a muffle furnace under oxygen atmosphere with flow rate of 60 sccm, then heated to 500 °C with rate of 3 °C min⁻¹ and maintained at 500 °C for 2 h. Then it was cooled to room temperature with rate of 3 °C min⁻¹. Finally TiO_2 NTs were achieved.

2.2. Fabrication of MoS_2 -rods/ TiO_2 NTs

Coupling TiO_2 NTs with MoS_2 rods was realized by a facile hydrothermal reaction. As a typical synthesis, 0.88 g ammonium molybdate ($(\text{NH}_4)_6\text{Mo}_7\text{O}_{24} \cdot 4\text{H}_2\text{O}$) was dissolved in 20 mL of distilled water, then 2.64 g sodium sulfide ($\text{Na}_2\text{S} \cdot 9\text{H}_2\text{O}$) and 4 mL

concentrated hydrochloric acid were added. After the resulting solution was heated in a thermostat with stirring at 90 °C for half an hour, 20 mL distilled water with 0.7 g hydroxylamine hydrochloride ($\text{NH}_2\text{OH} \cdot \text{HCl}$) dissolving was injected and stirred for another 10 min. The resulting solution and the TiO_2 NTs substrate were transferred into a 50 mL stainless Teflon-lined autoclave and heated at 120 °C for 12 h, and then cooled to room temperature naturally. The hybrid material was washed several times with distilled water and acetone. Finally, the MoS_2 -rods/ TiO_2 NTs was obtained after dried in the vacuum.

The surface morphologies of the as-prepared samples were characterized by scanning electron microscopy (SEM, Philips XL30 FEG) with accelerated voltage of 20 kV. The crystalline structures were characterized by X-ray diffraction (XRD, Rigaku D/MAX-rA, Japan) using a diffractometer with $\text{Cu K}\alpha$ radiation, $\lambda = 1.54184\text{ \AA}$ in the range of $2\theta = 10\text{--}80^\circ$, scan rate of 4° min⁻¹. Surface compositions were detected by X-ray photoelectron spectroscopy (XPS, ESCALAB 250) with a monochromated X-ray source ($\text{Al K}\alpha$ $h\nu = 1486.6\text{ eV}$). The UV-vis diffuse reflection spectrum (UV-vis DRS) was measured for photochemical properties using an IS19-1 in combination with a single reflection internal accessory (Beijing Purkinje General Instrument Co., Ltd.). The electrochemical properties were measured by CHI660D potentiostat (Shanghai Chen hua Instrument Co., Ltd.).

2.3. PEEC reduction of CO_2

The properties of PEEC reduction of CO_2 were measured by CHI660D potentiostat in 0.1 mol L⁻¹ KHCO_3 . It was carried out in a three electrodes cell, where Pt plate and saturated calomel electrode (SCE) were used as the counter and reference electrodes, respectively. The as prepared electrode with an area of 4 cm² was employed as the working electrode. The sweep rate was 50 mV s⁻¹. Before experiment, plunged N_2 into KHCO_3 at the rate of 40 sccm for 30 min. After that, CO_2 was plunged for 30 min until it was saturated, then repeated the experiment. The samples were illuminated under visible light by a Xenon lamp with a band-pass filter ($\lambda \geq 420\text{ nm}$, 100 mW cm⁻²).

2.4. Products analysis

During the reduction of CO_2 , the products were analyzed by gas chromatography (GC-9A, Shimadzu). The GC was equipped with glass packed column (2 m, inner diameter 3 mm, Parapak Q, 80–100) and FID. The column was kept at 70 °C while the detector was at 200 °C. High purity N_2 worked as carrier gas with a flow rate of 30 sccm.

3. Results and discussion

The surface morphology of the prepared electrode is shown in Fig. 1a. It demonstrates that MoS_2 grows to be hexagonal prism structure (length of 50–80 μm), and grows randomly on the surface of TiO_2 NTs. And the TiO_2 NTs can be seen from the gap of MoS_2 . Fig. 1b shows that the prepared TiO_2 NTs pile together with almost homogenous diameters (90–100 nm). Fig. 1c and d is the further enlarged images of MoS_2 , it can be clearly seen that they are hexagonal prism structure and their diameters are about 5 μm. Furthermore, surface morphologies on the MoS_2 are rather flat without notable defects. It is reasonable to imagine that the regular structure would be beneficial to the electron transfer, which is further favorable to improve the catalytic ability.

The crystal structure of the prepared MoS_2 -rods/ TiO_2 NTs is studied by XRD. Fig. 2 shows the XRD patterns of the MoS_2 -rods/ TiO_2 NTs, as well as that of the TiO_2 NTs. All diffraction peaks

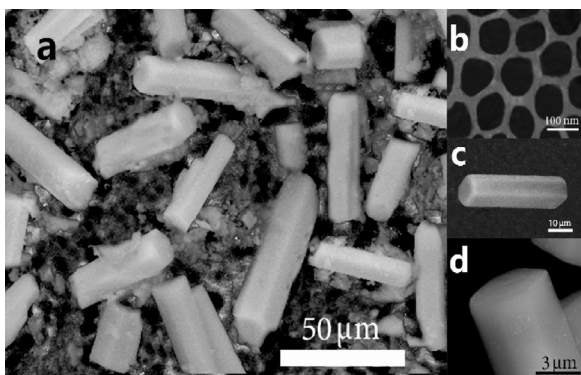


Fig. 1. SEM images of (a) MoS₂-rods/TiO₂ NTs, (b) TiO₂ NTs, (c) and (d) MoS₂ rods.

of TiO₂ NTs are still present in the XRD pattern of the MoS₂-rods/TiO₂ NTs, indicating that the intrinsic structure of TiO₂ NTs are not destroyed during the fabrication of MoS₂-rods/TiO₂ NTs. Moreover, it can be noted that the XRD pattern of MoS₂ included three main diffraction peaks, i.e., 2θ of 15.90° , 34.58° and 44.03° , which corresponded to the crystal faces of (0 0 2), (1 0 0) and (0 0 6). We calculate the lattice parameters $a = 3.1596 \text{ \AA}$ and $c = 12.3146 \text{ \AA}$, which is consistent with the JCPDS card (No. 37-1492). The strong

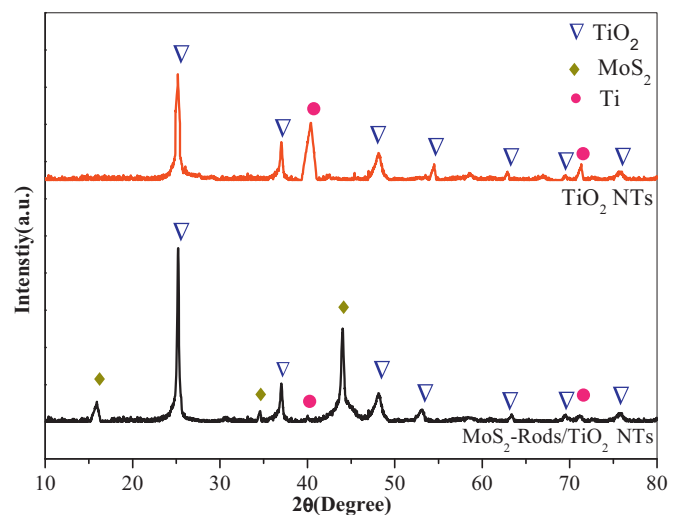


Fig. 2. XRD patterns of TiO₂ NTs and MoS₂-rods/TiO₂ NTs.

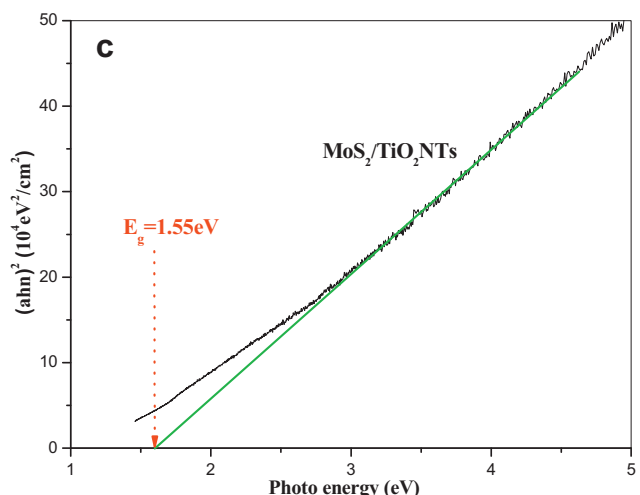
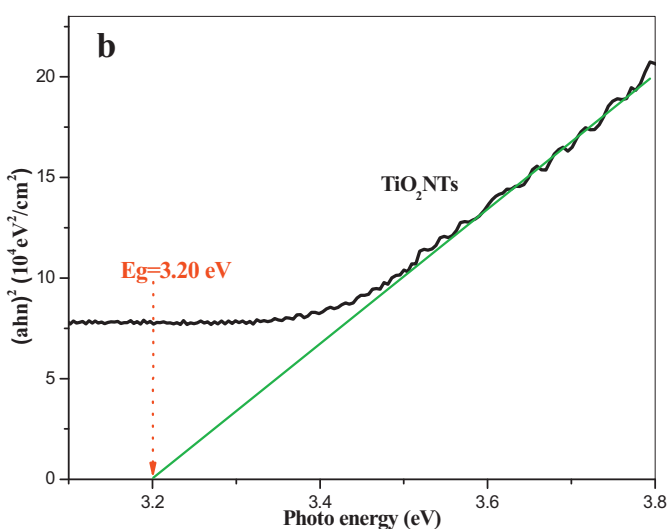
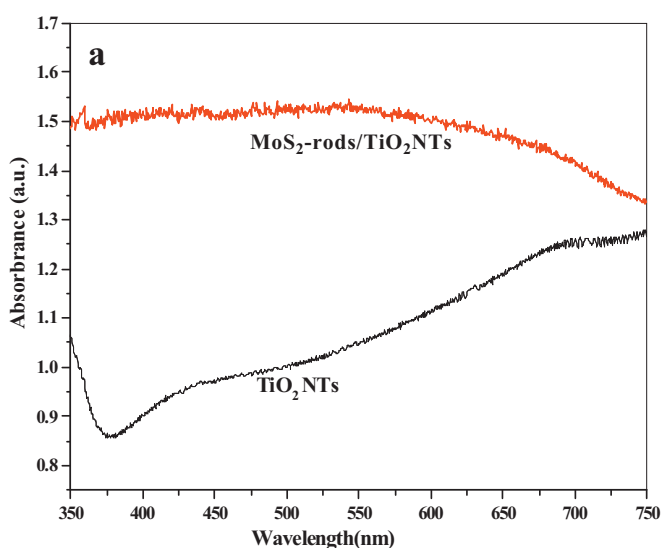


Fig. 3. (a) UV-vis DRS spectra of TiO₂ NTs and MoS₂-rods/TiO₂ NTs. (b) and (c) Plot analysis of optical band gap of TiO₂ NTs and MoS₂-rods/TiO₂ NTs.

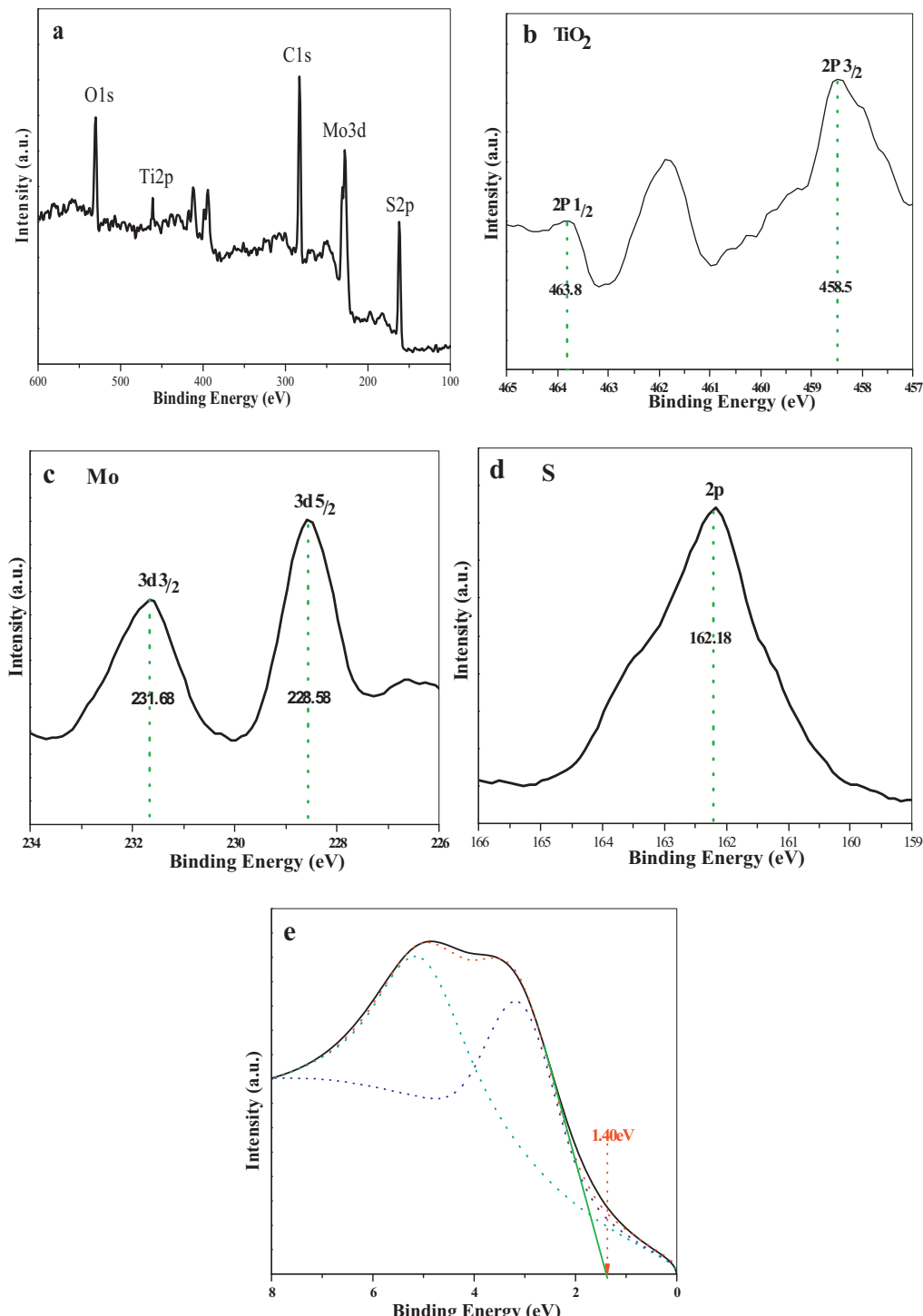


Fig. 4. XPS spectra of the composites. (a) The wide scan XPS spectrum of the MoS₂-rods/TiO₂ NTs. (b)–(d) Ti 2p, Mo 3d and S 2p XPS spectrum. (e) Valence band photoemission spectrum (solid line) and Gaussian fit (dashed line) of MoS₂-rods/TiO₂ NTs. The spectrum was smoothed and baseline corrected.

and sharp diffraction peaks indicate good crystallizations [18]. All the XRD peaks in Fig. 2 can be indexed to anatase TiO₂ and hexagonal system MoS₂, indicating that possible new phases, such as TiS₂, MoS, and MoO₂, are not formed. The findings along with the SEM confirm that the MoS₂-rods/TiO₂ NTs composite are successfully prepared.

The optical property of TiO₂ NTs and MoS₂-rods/TiO₂ NTs are determined by UV-vis DRS. Compared with TiO₂ NTs, the obtained MoS₂-rods/TiO₂ NTs exhibits a higher absorption in the visible area (400–600 nm), which proves that the optical absorption of the

material is enhanced greatly by the introduction of MoS₂-rods, as shown in Fig. 3a. The energy band gap (E_g) can be estimated by the conventional Tauc equation [19,20]:

$$\alpha h\nu = A(h\nu - E_g)^n \quad (1)$$

where $h\nu$ is the photon energy; α is the absorption coefficient; A is the constant; $n = 2$ for an indirectly allowed transition and $n = 1/2$ for a directly allowed transition. The E_g of MoS₂-rods/TiO₂ NTs (Fig. 3c) is 1.55 eV, whereas the E_g of TiO₂ NTs is 3.20 eV (Fig. 3b), which

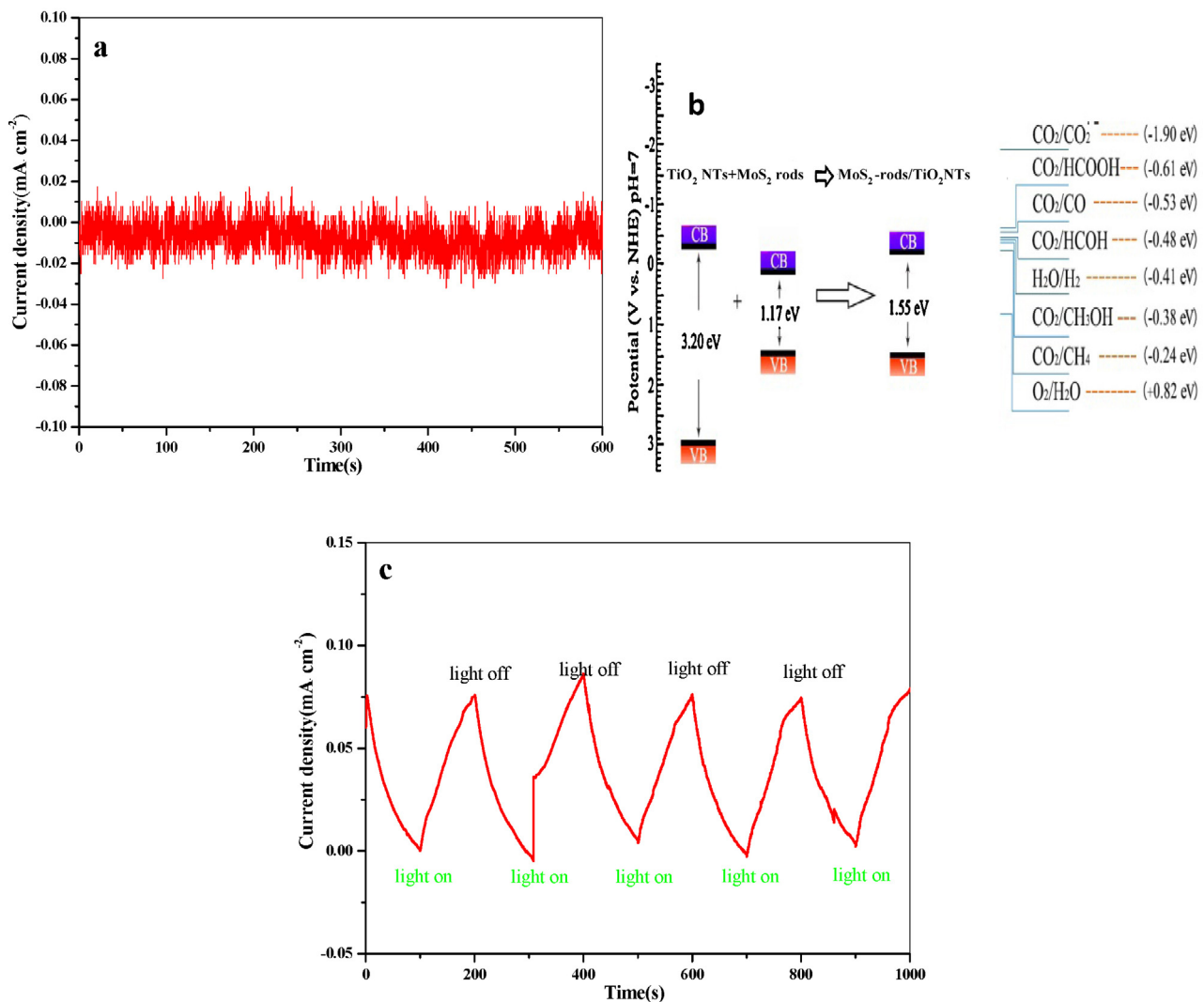


Fig. 5. (a) Photocurrent response behavior of MoS_2 -rods/ TiO_2 NTs. (b) Conduction band and valence band potentials of TiO_2 , MoS_2 , and MoS_2 -rods/ TiO_2 NTs relative to energy levels of the redox couples in water. (c) Current density difference value with time change under open circuit potential and illumination of simulated sunlight.

indicates the as-prepared materials could be excited and utilized by light with lower energy ($\lambda \leq 800 \text{ nm}$).

XPS is used to investigate the chemical components and the states of Mo and S in the MoS_2 -rods/ TiO_2 NTs heterostructure. The wide scan XPS spectrum (Fig. 4a) reveals that the predominant elements are Ti, O, Mo, S and C. Among these elements, Ti, O, Mo and S elements are from the prepared composites and the C element is from the XPS instrument itself. No other hetero-elements are detected. The molar ratio of MoS_2 and TiO_2 is about 4:1 obtained from the XPS [21]. The high-resolution XPS spectra (Fig. 4b-d) show that the binding energies of $\text{Ti } 2\text{p}_{1/2}$, $\text{Ti } 2\text{p}_{3/2}$, $\text{Mo } 3\text{d}_{3/2}$, $\text{Mo } 3\text{d}_{5/2}$ and $\text{S } 2\text{p}$ peaks are located at 463.80, 458.50, 231.68, 228.58 and 162.18 eV, respectively, suggesting that the prepared materials are consisted of Mo^{4+} , S^{2-} and Ti^{4+} . Fig. 4e shows the valence band photoemission spectrum of MoS_2 -rods/ TiO_2 NTs and its Gaussian fit. There are two distinguished peaks which are attributed to the electron emission from π (non-bonding) and s (bonding) O 2p orbital, respectively. The location of the valence band maximum (VBM) is about 1.40 eV determined directly from the electron emission spectrum by methods of a linear extrapolation [22,23]. With a calculated band gap of 1.55 eV by UV-vis DRS, we can deduce that the CBM is located at -0.15 eV.

The MoS_2 -rods/ TiO_2 NTs ability for photocatalytic reduction of CO_2 is studied by $I-t$ curve under open circuit potential and illumination of simulated sunlight in the CO_2 -saturated and N_2 -saturated 0.1 mol L^{-1} KHCO_3 aqueous solution. There are two main factors that increase the current density (I_{total}), one is the redox of H_2O ($I_{\text{H}_2\text{O}}$), and the other is the reduction of CO_2 (I_{CO_2}) to organic compounds. In order to eliminate the influence of redox of H_2O , we use the solution saturated with N_2 as comparison.

$$I_{\text{CO}_2} = I_{\text{total}} - I_{\text{H}_2\text{O}} \quad (2)$$

The I_{CO_2} is almost zero under open circuit potential and illumination of simulated sunlight, as shown in Fig. 5a. This fully proved the prepared MoS_2 -rods/ TiO_2 NTs has no PC reduction ability for CO_2 . Fig. 5b shows a schematic of the band-edge positions of the TiO_2 , MoS_2 , and MoS_2 -rods/ TiO_2 NTs with respect to the redox potentials of CO_2 [11]. The CBM of MoS_2 -rods/ TiO_2 NTs (-0.15 eV) is more positive than the CO_2 reduction potential, which reply why the prepared MoS_2 -rods/ TiO_2 NTs has no PC reduction ability for CO_2 .

Fig. 5c shows the photo-current and dark-current transients on the electrode MoS_2 -rods/ TiO_2 NTs in 0.1 mol L^{-1} KHCO_3 saturated with N_2 at open circuit potential. The photocurrent density (0.075 mA cm^{-2}) has a significant increase compared with the dark

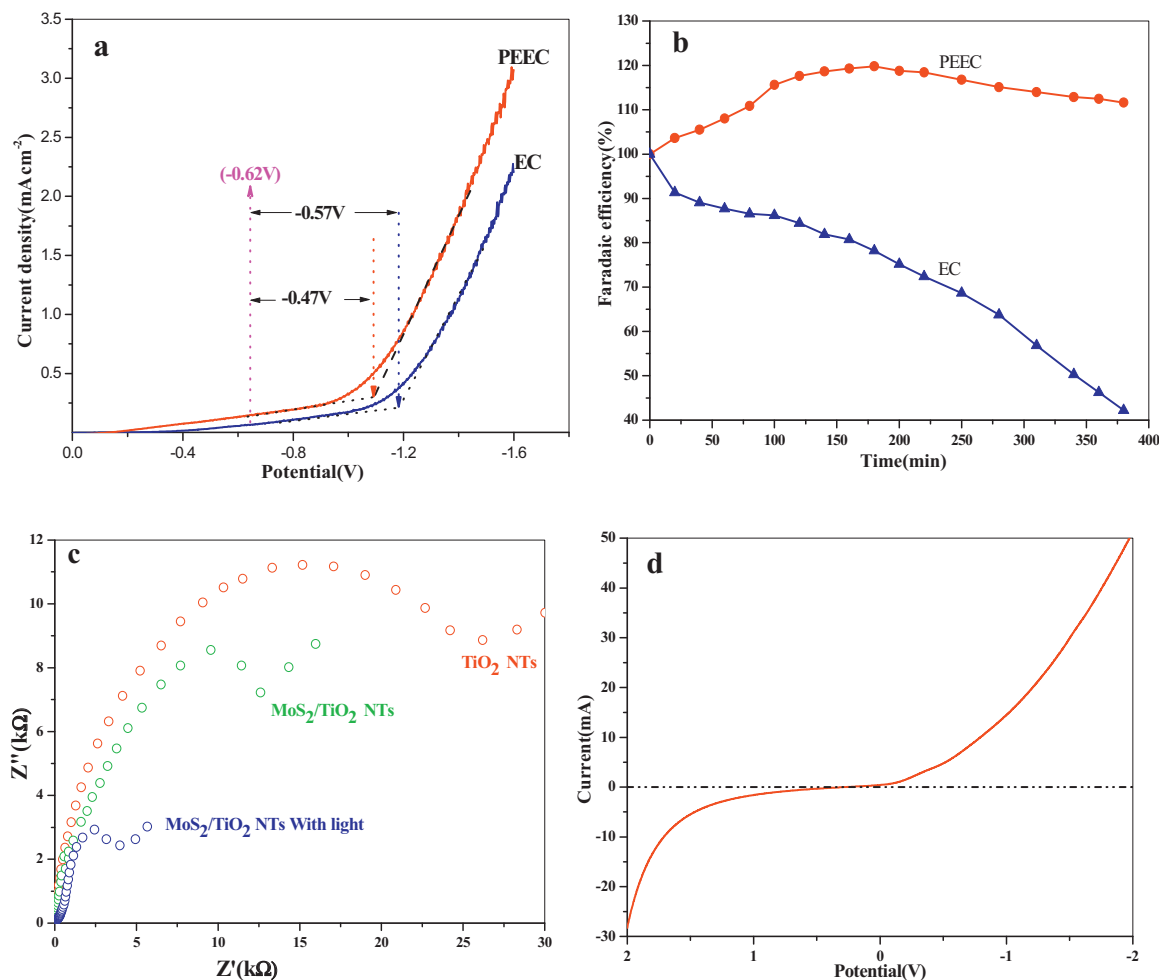


Fig. 6. (a) Current density difference value changing curves with potential. (b) Faradaic efficiency-T characteristic of the MoS₂-rods/TiO₂ NTs. (c) Electrochemical impedance spectroscopy of TiO₂ NTs, MoS₂-rods/TiO₂ NTs and MoS₂-rods/TiO₂ NTs under light. (d) Current density (*I*)-potential (*E*) characteristic of the MoS₂-rods/TiO₂ NTs. All runs were recorded in an aqueous KHCO₃ electrolyte solution (0.1 M, pH 7) with or without light illumination (100 mW cm⁻²) at 25 °C.

current density (almost zero) under visible light irradiation, which probably attributes to the reduction of H₂O to H₂ or/and the oxidation of H₂O to O₂. It can be seen from Fig. 5b that the VBM (1.40 eV) is much more positive than H₂O/O₂ oxidation potential (0.82 V), and the CBM (-0.15 eV) is more positive than H₂O/H₂ reduction potential (-0.41 V). According to the principle of the reduction of CO₂, this proves that the increase of current densities (Fig. 5c) owes to the oxidation of H₂O to O₂ rather than the reduction of H₂O to H₂. Here, MoS₂-rods/TiO₂ NTs exhibits a very interesting phenomenon, that is: it has no PC reduction ability for CO₂, but it can produce hydrogen proton in the H₂O photooxidative process, which is very helpful for CO₂ reduction to alcohols.

The linear sweep voltammetry (LSV) is conducted in 0.1 mol L⁻¹ KHCO₃ solution with a standard three-electrode configuration. Fig. 6a shows that the current density (*I*_{CO₂) changes with potential. The *I*_{CO₂ under EC gradually increased from -0.4 V to -1.2 V and mushroomed from -1.2 V, which indicates that the prepared electrode can process the electrocatalytic reduction of CO₂. However, in common with other electrocatalysts, the faradaic efficiency [24] of the prepared MoS₂-rods/TiO₂ NTs gradually reduced. As the EC line shown in Fig. 6b, the faradaic efficiency tends to drop off with time going on.}}

Faradaic efficiency

$$= \frac{\text{moles} \times \text{number of electrons needed for conversion}}{\text{moles of electrons passed}} \quad (3)$$

However, when we add illumination into the electrocatalysis systems, the faradaic efficiency does not decrease but slightly increases instead. As the PEEC line shown in Fig. 6b, the faradaic efficiency firstly increases gradually (0–200 min) and then declines slightly (200–380 min). Although the faradaic efficiency has a slight decrease, it still greater than 100 and far more than EC. After 380 min, the faradaic efficiency of PEEC (111.58%) is 2.65 times higher than that of EC (42.20%). The three reasons for how photo-enhance EC reduction of CO₂ are systematically investigated.

Firstly, the overpotential of reducing CO₂ decreased from -0.57 V (EC) to -0.47 V (PEEC) after introduction of light, as shown in Fig. 6a. The decreased overpotential can make the reaction easier. It also can be seen that *I*_(PEEC) is greater than *I*_(EC), which indicates that the photo-enhanced electrocatalysis of CO₂ generates (Fig. 6b).

Secondly, the introduction of light further improved the electron transmission ability. Fig. 6c shows the electrochemical impedance of TiO₂ NTs and MoS₂-rods/TiO₂ NTs is 25.0 kΩ and 12.7 kΩ, respectively. The electrochemical impedance of MoS₂-rods/TiO₂ NTs under light is 3.6 kΩ. It proves that the introduction of MoS₂ and light decreased the resistance of the TiO₂ NTs substrate, it strengthens the electron transfer velocity of the catalyst [25,26].

Finally the formation of heterojunction can further improve the reduction of CO₂. Fig. 6d illustrates the *I*-*V* characteristics of the MoS₂/TiO₂ NTs. The current increases exponentially under a negative bias, while in the positive region, the reverse current remains very limited. The obvious current asymmetry under the negative

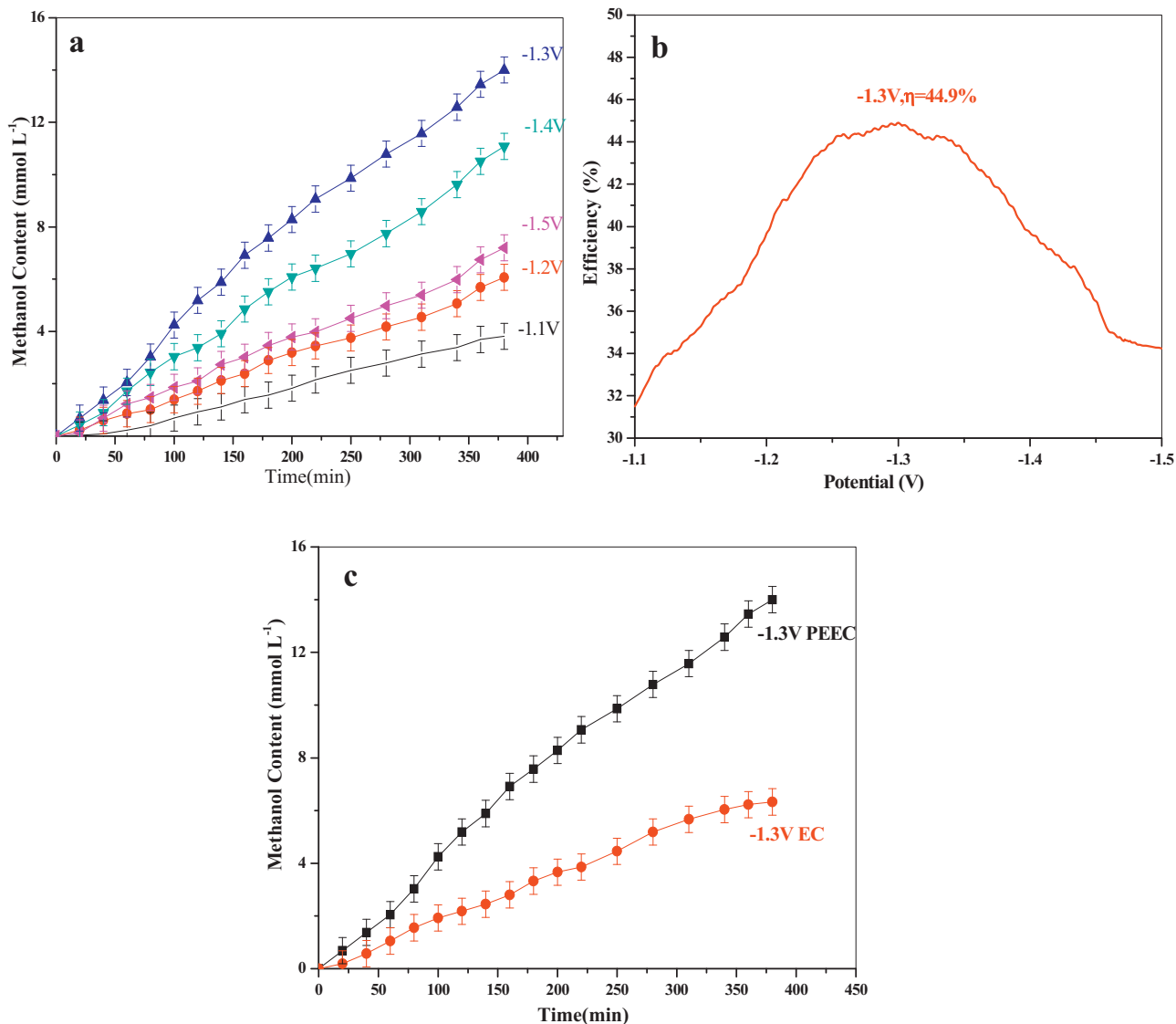
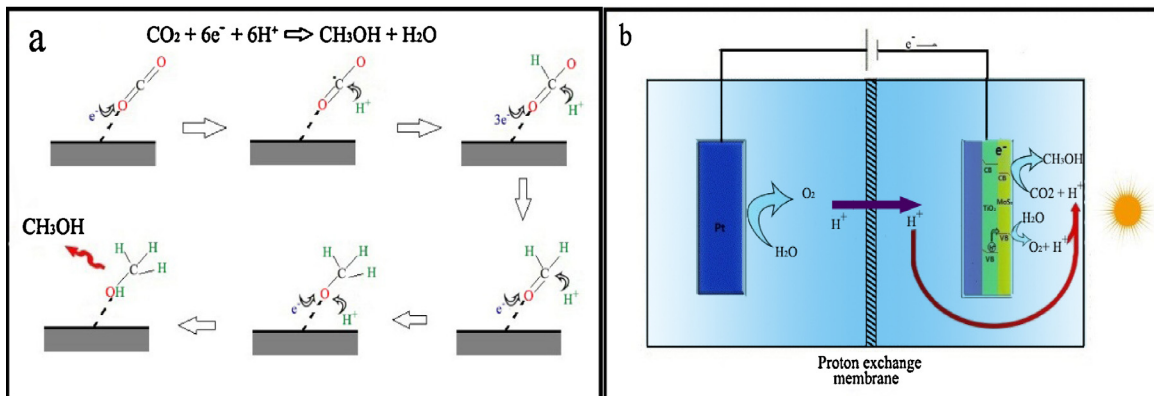


Fig. 7. Time dependence of the amount of methanol evolved from CO₂ PEEC reduction under visible light with different potentials (a) and under -1.3 V PEEC, -1.3 V EC and individual PC (c) in 0.1 mol L⁻¹ KHCO₃. (b) Current transformation efficiency of MoS₂-rods/TiO₂ NTs during PEEC CO₂ reduction.

and positive bias indicates the formation of p-n heterojunction between MoS₂-rods and TiO₂ NTs [27]. Existing p-n heterojunction helps to form an internal electric field and so further speed up electron transmission. On the other side, the internal electric

field is beneficial to the separation of photogenerated electrons and holes, thereby enhances internal PC oxidation water [28,29]. The H₂O photooxidative process offers protons which is used for CO₂ reduction, further improves the faradaic efficiency.



Scheme 1. Probable speculation reaction pathway for reduction of CO₂ into CH₃OH and the mechanism of the PEEC reducing CO₂ process on MoS₂-rods/TiO₂ NTs electrode.

The major PEEC product was methanol by GC analysing, and a small quantity of methane generated (the maximum methane yield of PEEC was 0.44 mmol L^{-1} after 6 h), so we mainly expanded discussion on the methanol in the following. As shown in Fig. 7a, with the potential changing from -1.1 V to -1.5 V , methanol yield increased firstly and then decreased and it reached the peak at -1.3 V , where there was the largest photoelectric current transformation efficiency ($\eta = 44.9\%$) of the system (Fig. 7b), the current transformation efficiency (η) was calculated as follows:

$$\eta = \frac{I_{\text{CO}_2} - I_{\text{N}_2}}{I_{\text{CO}_2}} \times 100\% \quad (4)$$

I_{CO_2} is the current density of PEEC reduction CO_2 , I_{N_2} is the current density of the solution saturated with N_2 under photoelectric conditions. Being consistent with the LSV, in the range of 0 to -1.3 V , the main reaction was CO_2 reduction. So with the potential toward to more negative, CO_2 reduction strengthened gradually. When the potential reached -1.3 V , PEEC CO_2 reduction reached the optimum and the yield of methanol reached a peak. While the potential was more negative than -1.3 V , hydrogen evolution reaction became the main reaction. And then the catalytic reduction efficiency of CO_2 and the methanol yield decreased.

In the experiment, there is no methanol produced during individual PC reduction, which is consistent with the unmatched energy band of the material. Individual EC reduction could reduce CO_2 to CH_3OH , but the yield was relatively low (Fig. 7c), and the faradaic efficiency gradually decreased with time (Fig. 6b, EC). PEEC reduction was much more efficient compared with mere EC. And the maximum methanol yield of PEEC was $14.49 \text{ mmol L}^{-1}$ after 6 h, 2.29 times higher than that of EC (6.32 mmol L^{-1}), which further illustrated the introduction of light greatly enhanced the reduction of CO_2 .

Based on these experimental results and literature reports, we propose a novel mechanism for the PEEC reduction of CO_2 to methanol. The reduction of CO_2 to CH_3OH is six electronic reactions, specific reaction as shown in Scheme 1a. At the initial stage, the CO_2 molecules are adsorbed onto the electrode surface by electrosorption. The adsorbed CO_2^- radical anion was formed during the first electronic reaction. Furthermore, it underwent a protonation to produce adsorbed CHO_2 as the key intermediate. By a succession of five protonation/electronation steps, the CH_3OH formed.

What is the special explanation is where the electron and hydrogen proton comes from, as shown in Scheme 1b. Since the MoS_2 -rods/ TiO_2 NTs has unmatched conductive band for PC reduction of CO_2 . Therefore, we believe that electrons for the reduction of CO_2 are just derived from the applied voltage. For the protons, we think that they come from two aspects. One side, when apply -1.3 V potential on the cathode, the anode potential is 1.82 V vs SCE, which has enough EC ability to oxidize water to oxygen and protons. Then the generated protons will arrive at the cathode involving into the CO_2 EC reduction reaction. On the other hand, the MoS_2 -rods/ TiO_2 NTs has appropriate valence band (1.40 eV) for in situ PC oxidation water to generate protons. Thus it provided more protons for EC reduction of CO_2 , which was one of the main reasons for the light greatly enhanced EC reduction of CO_2 .

4. Conclusions

MoS_2 -rods were hexagonal prism structure (length of $50\text{--}80 \mu\text{m}$) which were synthesized by a facile hydrothermal reaction, and then assembled MoS_2 -rods onto the TiO_2 NTs (obtained by improved potentiostatic anodic oxidation). Although, the obtained MoS_2 -rods/ TiO_2 NTs exhibited excellent optical

performance, it had an unmatched CBM (-0.15 eV) and individual EC had a low faraday efficiency. So we designed a new PEEC way to reduce CO_2 to methanol on MoS_2 -rods/ TiO_2 NTs. And it achieved obvious improvement on the faradaic efficiency and methanol yield after applying illumination. Besides, we introduced a special mechanism for the PEEC reduction of CO_2 to methanol on MoS_2 -rods/ TiO_2 NTs. And it is the first time to elaborate where the hydrogen proton and electron come from. With more complete knowledge of the PEEC, one can aspire to design catalysts capable of reducing CO_2 to methanol and other desired products selectively and efficiently. The technology to PEEC reduction of CO_2 to methanol and other industrial chemicals would be a significant step toward a more bright future.

Acknowledgements

This research was supported by the National Natural Science Foundation of China (Grant No. 21203114), Key Projects in the National Science & Technology Pillar Program during the Twelfth Five-year Plan Period (Grant No. 2011BAD11B01), and Promotive Research Fund for Excellent Young and Middle-aged Scientists of Shandong Province (Grant No. BS2012NJ008). We are grateful to the foundation supported by Shandong Jingbo Holdings Corporation.

References

- [1] V.P. Indrakanti, J.D. Kubicki, H.H. Schobert, Energy Environ. Sci. 2 (2009) 745–758.
- [2] K. Mori, H. Yamashita, M. Anpo, RSC Adv. 2 (2012) 3165–3172.
- [3] C.D. Windle, R.N. Perutz, Coord. Chem. Rev. 256 (2012) 2562–2570.
- [4] H.C. Hsu, I. Shown, H.Y. Wei, Y.C. Chang, H.Y. Du, Y.G. Lin, C.A. Tseng, C.H. Wang, L.C. Chen, Y.C. Lin, K.H. Chen, Nanoscale 5 (2013) 262–268.
- [5] M. Le, M. Ren, Z. Zhang, P.T. Sprunger, R.L. Kurtz, J.C. Flake, J. Electrochem. Soc. 158 (2011) E45–E49.
- [6] B.D. Yuhas, C. Prasittichai, J.T. Hupp, M.G. Kanatzidis, J. Am. Chem. Soc. 133 (2011) 15854–15857.
- [7] E.R.M. Ahmed, R. Sohrab, Energy Environ. Sci. 4 (2011) 1065–1086.
- [8] I. Tacchini, E. Terrado, A. Anson, M.T. Martinez, Micro Nano Lett. 6 (2011) 932–936.
- [9] P. Liu, Y.M. Choi, Y.X. Yang, M.G. White, J. Phys. Chem. A 114 (2010) 3888–3895.
- [10] X. Zong, G.P. Wu, H.J. Yan, G.J. Ma, J.Y. Shi, F.Y. Wen, L. Wang, C. Li, J. Phys. Chem. C 114 (2010) 1963–1968.
- [11] S.C. Roy, O.K. Varghese, M. Paulose, C.A. Grimes, Nano Lett. 3 (2010) 1259–1278.
- [12] N.S. Spinner, J.A. Vega, W.E. Mustain, Catal. Sci. Technol. 2 (2012) 19–28.
- [13] W. Tang, A.A. Peterson, A.S. Varela, Z.P. Jovanov, L. Bech, W.J. Durand, S. Dahl, J.K. Nørskov, I. Chorkendorff, Phys. Chem. Chem. Phys. 14 (2012) 76–81.
- [14] E.G.S. Firmino, M.A.L. Cordeiro, A.C. Rabelo, C.J. Dalmaschio, A.N. Pinheiro, E.C. Pereira, E.R. Leite, Chem. Commun. 48 (2012) 7687–7689.
- [15] V.W. Lau, A.F. Masters, A.M. Bond, T. Maschmeyer, Chem. Eur. J. 18 (2012) 8230–8239.
- [16] P.D. Tran, S.S. Pramana, V.S. Kale, M. Nguyen, S.Y. Chiam, S.K. Batabyal, L.H. Wong, J. Barber, J. Loo, Chem. Eur. J. 18 (2012) 13994–13999.
- [17] P.Q. Li, G.H. Zhao, X. Cui, Y.G. Zhang, Y.T. Tang, J. Phys. Chem. C 113 (2009) 2375–2383.
- [18] Z.H. Zhang, M.F. Hossain, T. Takahashi, Appl. Catal. B-Environ. 95 (2010) 423–429.
- [19] Y. Wang, Y. Zhang, G.H. Zhao, H.Y. Tian, H.J.T. Shi, C. Zhou, Appl. Mater. Interfaces 4 (2012) 3965–3972.
- [20] M.C. Acevedo, M.S. Faber, Y.Z. Tan, R.J. Hamers, S. Jin, Nano Lett. 12 (2012) 1977–1982.
- [21] D. Merki, H. Vrubel, L. Rovelli, S. Fierro, X. Hu, Chem. Sci. 3 (2012) 2515–2525.
- [22] N. Tsvetkov, L. Liudmila, S. Oleg, T.A. Byung, Energy Environ. Sci. 4 (2011) 1480–1486.
- [23] K.B. Debajeet, B. Artur, E. Rolf, F. Giuseppino, G. Thomas, C.C. Edwin, Chem. Mater. 23 (2011) 2051–2061.
- [24] B. Kumar, M. Llorente, J. Froehlich, T. Dang, A. Sathrum, C.P. Kubiak, Annu. Rev. Phys. Chem. 63 (2012) 541–569.
- [25] G. Wang, T. Liu, Y.J. Luo, Y. Zhao, Z.Y. Ren, J.B. Bai, H. Wang, J. Alloy Compd. 509 (2011) 216–221.
- [26] S.Q. Wang, X.Y. Jiang, H. Zheng, H.M. Wu, S.J. Kim, C.Q. Feng, NNL 4 (2012) 378–383.
- [27] C.W. Yi, T.H. Kim, W.Y. Jiao, Y. Yang, A. Lazarides, K. Hingerl, G. Bruno, A. Brown, M. Losurdo, Small 8 (2012) 2721–2730.
- [28] L.J. Yang, S. Wang, Q.S. Zeng, Z.Y. Zhang, L.M. Peng, Small 8 (2013) 1225–1236.
- [29] T.J. LaTempa, S. Rani, N.Z. Bao, C.A. Grimes, Nanoscale 4 (2012) 2245–2250.